# Reports

## Helicoidal Crack Propagation in Aluminous Orthoamphiboles

Abstract. *Sodic and aluminous orthoamphiboles from metamorphosed volcanic rocks develop helicoidal fractures upon cooling, due to elastic strain gradients radial to the* c-*axis. This condition may arise from radial composition gradients involving substitution of tetrahedral silicon by aluminum in the double chain structure or from intergranular boundary constraints with adjacent quartz.*

A comprehensive theory of three-dimensional crack propagation in anisotropic materials is essential to a complete understanding of brittle behavior. Since the pioneering efforts of Griffith (*1*), significant advances have come about with the recognition of submicroscopic defects and their role in the nucleation of cracks. When local stress concentrations attendant upon the buildup of dislocations on surfaces or grain boundaries exceed the minimum plastic yield strength of a crystal, a microcrack appears. The crack may then propagate through the crystal along the path of least resistance in response to the release of stored elastic energy. In the case of ideal brittle behavior, an existing crack will propagate when the elastic strain energy released on growth of the crack equals or exceeds the surface energy of the newly formed crack surface. Thus, the ability of a crack to extend its surface area by an additional amount will depend on the continued availability of elastic energy.

A relatively simple model by which the state of internal strain may change continuously with time is provided by differential thermal contraction. When the temperature of an anisotropic crystal is raised or lowered uniformly, it will undergo homogeneous elastic strain due to a continuous change in the interatomic distances and rotation of interatomic vectors. As long as no discontinuous phase changes occur, the lattice will deform in a continuous manner. In the case of an orthorhombic crystal, the principal components of the strain ellipsoid at any temperature are given by the linear coefficients of thermal expansion in the *a*, *b*, and *c* crystallographic directions. Because the symmetry of the ellipsoid must be consistent with the point group symmetry of the crystal, one can expect the principal components of strain to change in magnitude but not in direction with respect to the crystallographic axes.

In metamorphic rocks, thermal contraction will commonly force readjustments along grain boundaries as the molar volumes of the various minerals change. In special circumstances where movement along grain boundaries is constrained, the resulting elastic energy may be released by the formation of intracrystalline cracks. As these cracks are likely to propagate as cooling proceeds, their geometry may provide a useful record of strain history.

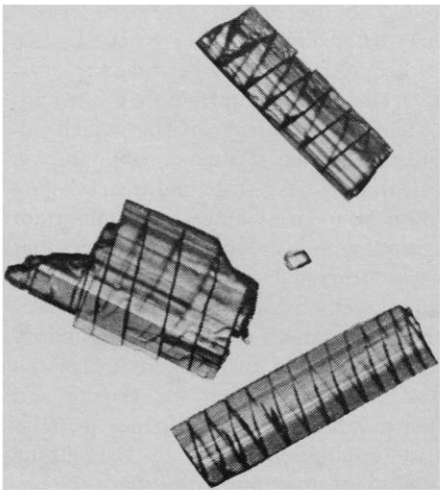

Fig. 1. Helicoidal cracks in naturally deformed gedrite. The crystals were photographed through a microscope in oil (refractive index 1.55) (× 333).

A geologic example for which these general principles may apply is provided by specimens of sodic and aluminous orthoamphiboles (gedrite) collected from regionally metamorphosed volcanic rocks near Keene, New Hampshire. Gedrite comprises approximately 70 percent by volume of each specimen studied, with quartz (20 percent), cordierite, and garnet present in lesser amounts. All phases have apparently equilibrated in the sillimanite zone at approximately 600° to 700°C and 5 to 6 kbar. The rocks have subsequently cooled, and the gedrite now exhibits a variety of brittle cracks, the most striking of which are shown in Fig. 1. In adjacent rocks, more aluminous orthoamphiboles and calcic monoclinic amphiboles recrystallized under the same conditions exhibit pervasive exsolution in response to chemical and mechanical readjustment to the cooling event (*2*).

Examination of gedrite single crystals in oil immersion and in polished sections indicates that minimum yield strengths are most frequently attained in or near the (001) plane. This direction is normal to the alternating double silica tetrahedral chains and octahedral strips and normal to the direction of morphologic elongation. Sets of parallel cracks or partings divide single crystals into segments which exhibit no relative lattice disruption. This is readily confirmed by the uniform parallel extinction in polarized light in all [001] zone sections. In monomineralic zones comprised of many homoaxial intergrowths, such cracks commonly extend across grain boundaries. In the case where quartz is present and separating amphibole grains, cracks are normally terminated at grain boundaries. In all specimens observed, quartz intergrown with amphibole is uncracked and free of strain shadows commonly associated with elastic strain.

Parallel cracks of this kind appear to nucleate at amphibole-quartz grain boundaries. Upon nucleation, the cracks propagate inward either to be terminated against tiny breaks parallel to the *c*-axis or to penetrate the entire diameter of the crystal as closed surfaces. The fracture surfaces shown in Fig. 1 are

---

*Scoreboard for Reports*: In the past few weeks the editors have received an average of 68 Reports per week and have accepted 12 (17 percent). We plan to accept about 12 reports per week for the next several weeks. In the selection of papers to be published we must deal with several factors: the number of good papers submitted, the number of accepted papers that have not yet been published, the balance of subjects, and length of individual papers.

Authors of Reports published in *Science* find that their results receive good attention from an interdisciplinary audience. Most contributors send us excellent papers that meet high scientific standards. We seek to publish papers on a wide range of subjects, but financial limitations restrict the number of Reports published to about 15 per week. Certain fields are overrepresented. In order to achieve better balance of content, the acceptance rate of items dealing with physical science will be greater than average.

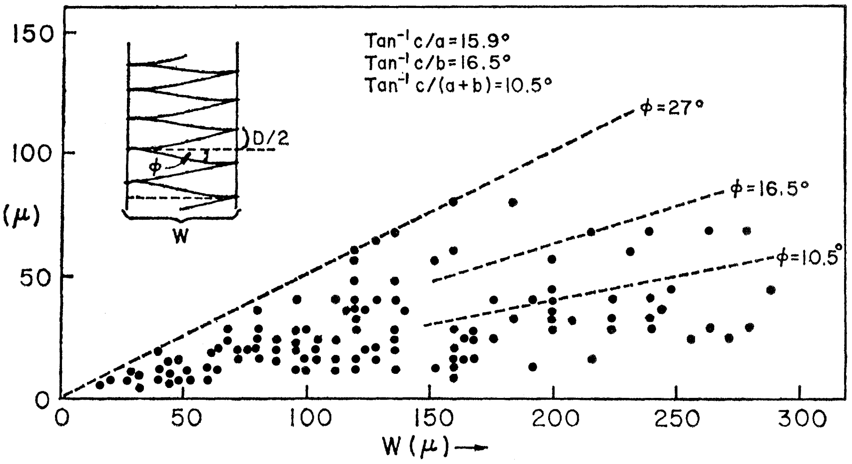

Fig. 2. Plot of one-half the pitch interval against width for helicoidal cracks measured in single gedrite crystals.

similar, but are characterized in addition by a substantial climb component in the crystallographic *c* direction. The surface defines a helicoid or helical ramp whose axis corresponds exactly to the 5.28-Å lattice repeat direction. The plane perpendicular to the helicoid axis is (001), with unit cell translations $a = 18.60$ Å and $b = 17.84$ Å (*3*). Any line normal to the *c*-axis and on the helical surface terminates at or near the geometric center of sections normal to *c*. It is for this reason that the three-dimensional form of the helicoids is not readily apparent in typical cleavage fragments prepared for oil immersion study. Most amphibole crystals break along the (110) cleavage direction parallel to the length of the crystal. In general, only the rodlike fragments that contain the central axis of the helicoid will exhibit the full helicoid symmetry. Other cleavage fragments will show parallel sigmoidal fracture patterns whose curvature depends on the shape and orientation of the fragment. Both left- and right-handed helicoids occur in approximately equal numbers.

Comparative x-ray diffraction studies on single gedrite crystals with and without helicoidal cracks show identical patterns. The absence of relative lattice rotation suggests that the mechanism by which the helicoids propagate is such that lattice registry is preserved. The data shown in Fig. 2 characterize the propagation paths of helicoidal cracks on the basis of pitch interval (*D*) and width (*W*) measured on single crystals. The ratio of these parameters gives the ratio of the climb component parallel to the *c* translation direction to the component in the crystallographic *ab* plane. The range of pitch angles observed from 130 grains is from approximately 4° to 27°. These may be accounted for by integral unit cell translations between $2(a + b) + c$ and $a + 2c$, corresponding to pitch angles of 4.14° and 29.6°, respectively. Unit cell translations of $b + c$, $a + c$, and $a + b + c$ generate pitch angles equal to the mean values indicated next to the dashed lines in Fig. 2.

Although there is some uncertainty (*4*) about the thermal expansion behavior of orthorhombic amphiboles, crack propagation symmetry suggests that the 5.3-Å direction in gedrite is one of relative tension. The symmetry of helicoidal cracks and the fact that microcracks commonly propagate inward from grain boundaries further suggest that the state of elastic strain before cracking is symmetric about the central axis of the crystal. There is evidence for at least two mechanisms by which an elastic strain gradient radial to the central axis of a crystal may be generated. First, the occurrence of helicoidal cracks is restricted to crystals enclosed in unfractured and apparently unstrained quartz, which indicates that the relative crystallographic orientations of gedrite and quartz along grain boundaries may be an important consideration. Polyphase fragments that show helicoidal gedrite interfaced with quartz demonstrate in these occurrences that the strength of the grain boundary locally exceeds that of either crystal. The extent to which the gedrite and quartz lattices register depends on relative orientation, and as the elastic moduli of the minerals differ, the resulting elastic strain in each grain upon cooling will be different. Given favorable registry, the gedrite lattice may be constrained at grain boundaries with quartz in such a manner that a radial strain gradient can be established.

Second, several of the larger gedrite crystals observed are compositionally zoned (*5*), from an aluminous and sodic core [$Na_{0.33}Fe_{2.80}Mg_{3.40}Al_{1.98}Si_{6.57}O_{22}(OH)_2$] outward to a less aluminous and sodic rim [$Na_{0.20}Fe_{2.80}Mg_{3.90}Al_{0.93}Si_{7.20}O_{22}(OH)_2$]. The chemical gradients are expressed optically by an elongate zone parallel to and including the central axis of each crystal. Such zones exhibit pronounced absorption in polarized light and pervasive exsolution parallel to (010). In contrast, the peripheral regions are colorless and free of visible exsolution. Compositional zoning is also observed in coexisting garnet, plagioclase, and gedrite from adjacent rocks and is believed to be due to prograde regional metamorphism. Hence, the zoning existed before the cooling event that presumably gave rise to the fractures.

The structural mechanism by which an elastic strain gradient is produced is related to the ionic substitutions deduced from the amphibole compositions given above and from other phases in the anthophyllite-gedrite series (*6*). Replacement of tetrahedral Si by Al and occupancy of the normally vacant "A" site (*7*) will decrease the average bond strength to bridging oxygens in the double tetrahedral chain. Lower excitation energies consequently result in greater elastic compliance parallel to the *c*-axis for the aluminous cores of zoned gedrite than for the less aluminous margins. This effect, however, may be compensated by the shortening of octahedral cation-oxygen bond lengths between the tetrahedral chains due to the substitution of Al for Mg in the M(2) site. The M(4) site occupancy is apparently unaffected by these substitutions and hence may not have the same importance as it has in the clinoamphiboles, or as the structurally analogous M(2) site has in the pyroxenes, for explaining the structural mechanisms of thermal expansion (*8*). In any case, the magnitude of the principal strain components is a function of chemical composition and thus thermal contraction or expansion will produce a strain gradient whose symmetry will conform to that of composition gradients.

JAMES H. STOUT
*Department of Geology and Geophysics,*
*University of Minnesota,*
*Minneapolis 55455*

**References and Notes**

1. A. A. Griffith, *Appl. Mech. Proc. 1st Int. Congr.* (1925), p. 55.
2. P. Robinson, *Trans. Am. Geophys. Union* **47**, 424 (1966). For other examples of typical exsolution phenomona see M. Ross, J. J. Papike, K. W. Shaw, *Mineral. Soc. Am. Spec. Pap. 2* (1969), p. 272; P. Robinson *et al.* (*6*).
3. Lattice parameters were determined by J. Braun from single crystal precession photographs obtained with Cu radiation and a Mo filter.
4. M. Wittels, *Am. Mineral.* **36**, 851 (1951).
5. Electron microprobe analyses were done on a Materials Analysis Company instrument with natural gedrite and anthophyllite standards, operating conditions, and reduction techniques as described in J. H. Stout, *J. Petrol.* **13**, 99 (1972).
6. P. Robinson, M. Ross, H. Jaffe, *Am. Mineral.* **56**, 1005 (1971).
7. J. J. Papike and M. Ross, *ibid.* **55**, 1945 (1970).
8. Y. Ohashi and C. W. Burnham, *ibid.* **58**, 843 (1973); M. Cameron, S. Sueno, C. T. Prewitt, J. J. Papike, *ibid.*, p. 594; J. R. Smyth, *ibid.*, p. 636.
9. Research supported by NSF grant GA 36092 and the Graduate School, University of Minnesota. I thank P. Hudleston for his penetrative review and numerous colleagues whose continued interest and curiosity stimulated this work.

2 April 1974

■

# Long-Lived Chemiluminescence in Cigarette Smoke

Abstract. *Cigarette smoke contains high concentrations of unstable molecules that react with oxygen to produce chemiluminescence. The chemiluminescent activity is concentrated in the aerosol phase that can be absorbed on glass-fiber filters and extracted into organic solvents. Cigarette smoke in* N,N-*dimethylformamide produces a long-lasting luminescence visible to the dark-adapted eye. We have demonstrated the oxygen dependence and have measured the kinetics, activation energies, emission spectra, and absolute photon intensities of this chemiluminescence. The total light emission from a single puff (35 cubic centimeters) of cigarette smoke is greater than $10^{12}$ photons. There was a significant correlation between smoke chemiluminescence and tar content. It is suggested that the chemical production of electronically excited states of aromatic hydrocarbons is equivalent to photoexcitation in the promotion of the carcinogenicity of these agents.*

If one has a phototube with good sensitivity and very low dark noise, it is possible to measure light emission from most chemical reactions and to a degree from most biological oxidations (*1, 2*). It was therefore of great interest to verify that a low-level luminescence issued from cigarette smoke exhaled into a glass vial (*3*).

We now report that this light emission is not a trivial process. Cigarette smoke contains high concentrations of unstable molecules that react with molecular oxygen to produce electronically excited states. Under proper conditions the photon yield of this chemiluminescence can be increased many orders of magnitude. The aerosol fraction of a single puff (35 $cm^3$) of cigarette smoke contains sufficient chemiluminescent precursors so that when they are extracted into organic solvents at 37°C a persistent chemiluminescence becomes visible to the dark-adapted eye.

Cigarettes were puffed (35 $cm^3$ in 2 seconds) through Whatman GF/C or GF/F glass-fiber filters mounted in Millipore Swinex-25 filter holders. The GF/C and GF/F glass-fiber filters and Millipore filters (pore size, 0.1 $\mu$m) were of essentially equal efficiency in collecting the portion of aerosol giving rise to the observed chemiluminescence. The filter was immediately removed from the holder, placed in 5 ml of organic solvent [*N,N*-dimethylformamide (DMF), dimethyl sulfoxide (DMSO), or dioxane] in a glass vial, and agitated for 30 seconds on a Vortex mixer. Chemiluminescent intensities were measured in calibrated photometer geometries with the use of d-c amplifier techniques and single photon counting. Absolute photon intensities were measured by direct comparison with a $^{14}C$-activated luminous reference source previously calibrated for the absolute photon emission of dinoflagellate bioluminescence (*4*). Measurements were also made in the liquid scintillation counter. The phototube gain was set for single photon counting and the counter was operated in the "coincidence off" mode (*5*). All operations were performed in the dark or in dim red light. The smoke extracts are subject to light-induced chemiluminescence. This is probably a pathway that could account for the reported photo-induced degradation of cigarette smoke extracts (*6*). Glassware, subject to considerable photo-excited phosphorescence, was also kept in darkness prior to use.

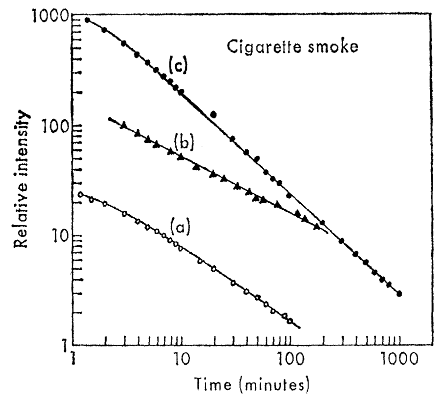

Fig. 1. Log-log plot of relative intensities of chemiluminescence versus time of (a) cigarette smoke aerosol deposited on a glass-fiber filter, (b) a 5-ml DMF extract of cigarette smoke, and (c) a 1 : 100 dilution of an initial extract. The relative scales apply to each curve separately and are not intended to compare the absolute photon intensities measured for (a), (b), and (c).

There is a requirement for molecular oxygen. Degassed smoke extracts in DMF and DMSO solvents were prepared under freezing and thawing conditions in a vacuum sufficient to observe a substantial photoreduction (bleaching) of aqueous solutions of flavin mononucleotide at 436 nm. Upon readmission of oxygen, chemiluminescent intensities of smoke extracts increased by factors of 20 to 50. A direct interaction with molecular oxygen would be consistent with the large free-energy requirements for chemical luminescence (*7*).

The apparent Arrhenius activation energies for smoke chemiluminescence in DMF, DMSO, and dioxane solvents were between 12 and 15 kcal $mole^{-1}$ in the temperature range from 10° to 60°C. It is also possible to collect smoke samples on glass-fiber filters, freeze them on Dry Ice, and reactivate the chemiluminescence a day or two later by inserting the filter into DMF at room temperature.

The reactions giving rise to the chemiluminescence are complex, as shown in Fig. 1, in which we have plotted the logarithm of chemiluminescent intensity as a function of logarithmic time for smoke aerosol on a glass-fiber filter and for smoke extracts in DMF solvent. For relative measurements of the chemiluminescence of smoke extracts we arbitrarily measured the intensity at 90 seconds after the delivery of the smoke sample to the glass-fiber filter. While the order of the chemiluminescent reaction was higher than first order with respect to time, the variation in chemiluminescent intensity with dilution was approximately linear below concentrations in which self-absorption in the